G-Band Micro-Fabricated Frequency-Steered Arrays With 2°/GHz Beam Steering

Leonardo Ranzani, *Member, IEEE*, Daniel Kuester, *Student Member, IEEE*, Kenneth J. Vanhille, *Member, IEEE*, Anatoliy Boryssenko, *Member, IEEE*, Erich Grossman, *Member, IEEE*, and Zoya Popović, *Fellow, IEEE*

***Abstract*—In this paper, we describe micro-fabricated frequency-scanned slot waveguide arrays operating between 130 and 180 GHz for planetary landing radar. The group delay dispersion of the feed line is increased by corrugating the bottom rectangular waveguide wall. Both 16-element and 32-element linear arrays are fed by micro-coaxial corporate feed networks to narrow the beam in the non-scanning direction. Two-dimensional (2-D) antenna arrays and feed networks are photo-lithographically fabricated using a sequential metal deposition process. The 16-by-21 array demonstrates a 6° beamwidth and 2°/GHz steering over a 40° scan angle.**

***Index Terms*—Beam steering, G-band, millimeter-wave radar, planar antenna arrays.**

I. Introduction

In STANDARD phased array antennas, phase shifters are typically used to control the direction of the main beam [1] and have been extensively used in communications and radar. Planetary landing radar, such as the ones recently used in the Curiosity mission to Mars, is a radar application where a phased array determines the height above the planet and the type of obstacles in the neighborhood of the landing site [2], [3]. A Ka-band phased array with 6 antennas, each 20 cm in diameter, totalling about 1.5 m×0.5 m×8 cm in size was used in this case [3], [4]. In order to reduce the size and mass for future planetary landing radar, the frequency can be increased to several hundred gigahertz, since the Mars atmosphere does not attenuate in this frequency range as much as the Earth's atmosphere.

Above W-band, phase shifters are nonexistent or lossy [5], and a frequency-scanned array requiring only a voltage-controlled oscillator (VCO), possibly with multipliers, becomes an attractive option [6]. However, large scan angles imply a broadband transmitter and receiver. Traveling-wave slotted dominant-mode rectangular waveguides have been used as frequency-scanned arrays at S-, X-, and Ka-bands, e.g., [7]–[11], with 10 ° of scanning for 10% fractional frequency bandwidth. In [12], a 130–180 GHz frequency scanned array was demonstrated with close to 1°/GHz of steering by use of a standard waveguide feed. When bandwidth is not available, e.g., in the unlicensed ISM 2.4-GHz band with an allowable bandwidth of only 4%, dispersion can be introduced as was demonstrated in [13] with bandpass filters, at the expense of increased loss. Here, we build on the work presented in [12], but with doubled scanning bandwidth, enabled by a microfabricated slow-wave structure inside the traveling-wave feed. This particular implementation enables dense packaging of parallel waveguides with radiating slots into a 2-D array aperture free of grating lobes in the visible space.

In our microfabricated arrays, the bottom wall of the waveguide is corrugated, while the slots are placed on the top wall at a half-wavelength period at the center frequency. Both 16- and 32-element linear arrays are fed with micro-coaxial corporate feeds, enabling beam-narrowing in the non-scanning direction. The 2-D arrays are fabricated by use of a wafer-scale sequential metal deposition process [14], and their radiation patterns are characterized in a quasi-optical setup.

In the next section, the design of the linear frequency scanning arrays is presented, along with the design of the feed network for the 2-D arrays. In Section III, the fabrication method is detailed, followed by a summary of the measurements of S-parameters and radiation patterns.

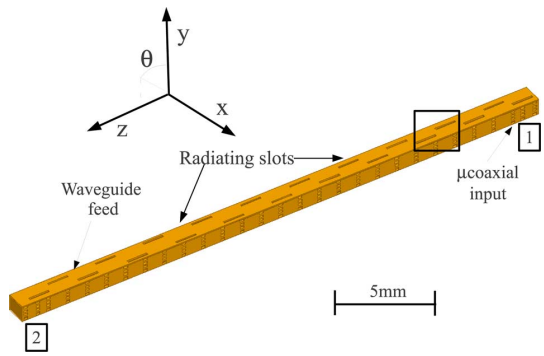

Fig. 1. Corrugated waveguide array geometry. The device is fed at port 1 from the bottom by a microfabricated coaxial line and terminated in a matched load at port 2. The corrugations are in the bottom waveguide wall. The spacing between adjacent slots is about half a wavelength at the center frequency.

II. Ridge Waveguide Antenna Array Design

The basic antenna array designed in this work is shown in Fig. 1. The lower waveguide wall has a corrugated ridge with a period d that is about $\lambda_0/10$ (λ_0 is the free-space wavelength) at

Manuscript received April 09, 2013; revised June 02, 2013; accepted June 17, 2013. Date of publication July 17, 2013; date of current version September 18, 2013. This work was supported by the National Aeronautics and Space Administration (NASA) under ContractNNX10CA77C.

D. Kuester, L. Ranzani, and Z. Popović are with the Department of Electrical and Computer Engineering, University of Colorado, Boulder, CO 80309 USA (e-mail: leonardo.ranzani@colorado.edu).

E. Grossman is with the National Institute of Standards and Technology, Boulder, CO 80303 USA.

K. Vanhille and A. Boryssenko are with Nuvotronics LLC, Radford, VA 24141 USA.

Color versions of one or more of the figures in this paper are available online at http://ieeexplore.ieee.org.

Digital Object Identifier 10.1109/TTHZ.2013.2271381

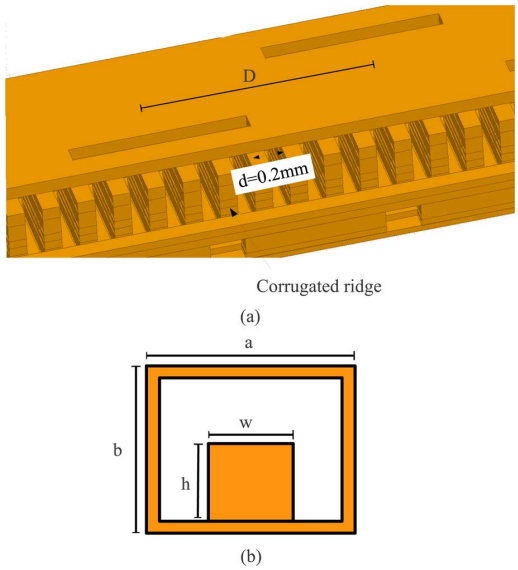

Fig. 2. (a) A detail of the ridge corrugations and the slot antennas from Fig. 1. (b) Cross section of the waveguide feed. The dimensions are $a = 800$ μm, $b = 675$ μm, $w = 500$ μm, $h = 375$ μm.

the center of the operating frequency band, as shown in Fig. 2. The distance D between longitudinal slots in the top wall is about $\lambda_0/2$ at the center frequency. The resulting traveling-wave array is fed by a microfabricated coaxial input and terminated in a matched impedance. The array beam scans in the H-plane, along the direction of the array, as the signal frequency varies over a large bandwidth.

The theory of periodically loaded microwave lines is discussed in [15], [16]. If a line is periodically loaded by sub-wavelength discontinuities, then Floquet–Bloch modes propagate in the structure and their propagation constant β_g is given by [15]:

$$\cos \beta_g d = \cos \beta_u d - \frac{b}{2} \sin \beta_u d \tag{1}$$

where β_u is the propagation constant in the uniform waveguide, d is the period of the discontinuities and b is the loading susceptance of the discontinuity, normalized to the characteristic impedance of the line. As a consequence of (1), the propagation constant β_g of the fundamental mode changes with frequency, thus increasing the scanning angle of the array. The scanning angle can be computed with the following formula [12]:

$$\sin \theta = \frac{\lambda_0}{\lambda_g} - \frac{\lambda_0}{2D} \tag{2}$$

where $\lambda_g = 2\pi/\beta_g$ and $\lambda_0 = 2\pi/\beta_0$ and D is the distance between subsequent slots. In the device described in this work a periodic discontinuity is obtained by modulating the height h of the waveguide ridge. The expected scan angle for a uniform slot array, as estimated by using (2), is shown in Fig. 3. The waveguide used in the simulations is $a = 800$ μm wide and $b = 675$ μm tall. The ridge in the uniform feedline is $w = 500$ μm wide and $h = 375$ μm tall. The period of the corrugation was $d = 200$ μm. The array scan angle per unit frequency increases with the waveguide wall corrugation depth, as visible in Fig. 3.

The radiating slot elements in the final device are 1 mm long and 0.1 mm wide. Standard slotted-waveguide design

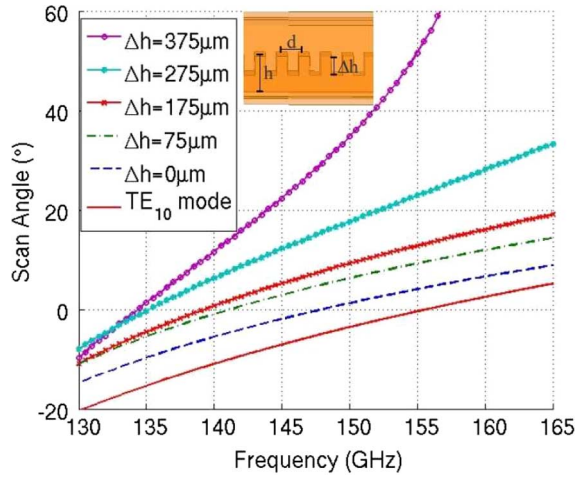

Fig. 3. Theoretical scan angle for different corrugation depths. The waveguide and ridge dimensions are reported in the caption of Fig. 2. The distance between the slots is assumed $d = 1.294$ μm. The line with the deepest corrugation, $\Delta h = 375$ μm, is used in the final design. The scan angle for the TE_{10} mode in a standard WR-5 rectangular waveguide is plotted for comparison.

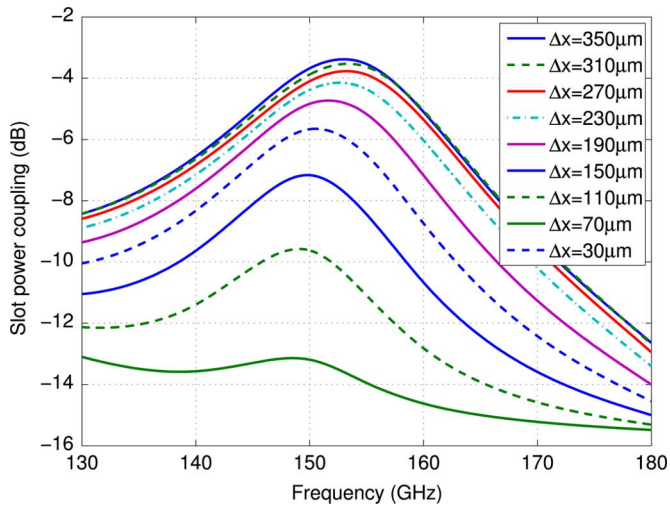

Fig. 4. Coupled power into a single longitudinal slot fed by a single-ridged waveguide as a function of frequency. The waveguide is 800 μm wide and 675 μm tall. The ridge is 500 μm wide and 375 μm tall. The slot offset Δx with respect to the feed center is controlled to tune the amount of coupling.

techniques were employed here to position the slots, in order to maximize gain and bandwidth. Following [17], the slot to slot distance is set to $\lambda_0/2$, where λ_0 is the signal free-space wavelength.

To synthesize the array aperture, an equivalent circuit representation for the radiating slots was adopted in this work. Initially full-wave simulations were employed to derive the equivalent circuit representation of a single slot. The power coupling for a single slot as a function of frequency and slot offset was simulated in HFSS™[1] and the result is shown in Fig. 4. The amount of coupling was extracted from the scattering parameters of a short waveguide section feeding a single slot and

[1]Certain commercial software, equipment, instruments, and materials are identified in this paper to foster understanding. Such identification does not imply recommendation or endorsement by the National Institute of Standards and Technology, nor does it imply that the software, the material, or the equipment are necessarily the best available for the purpose.

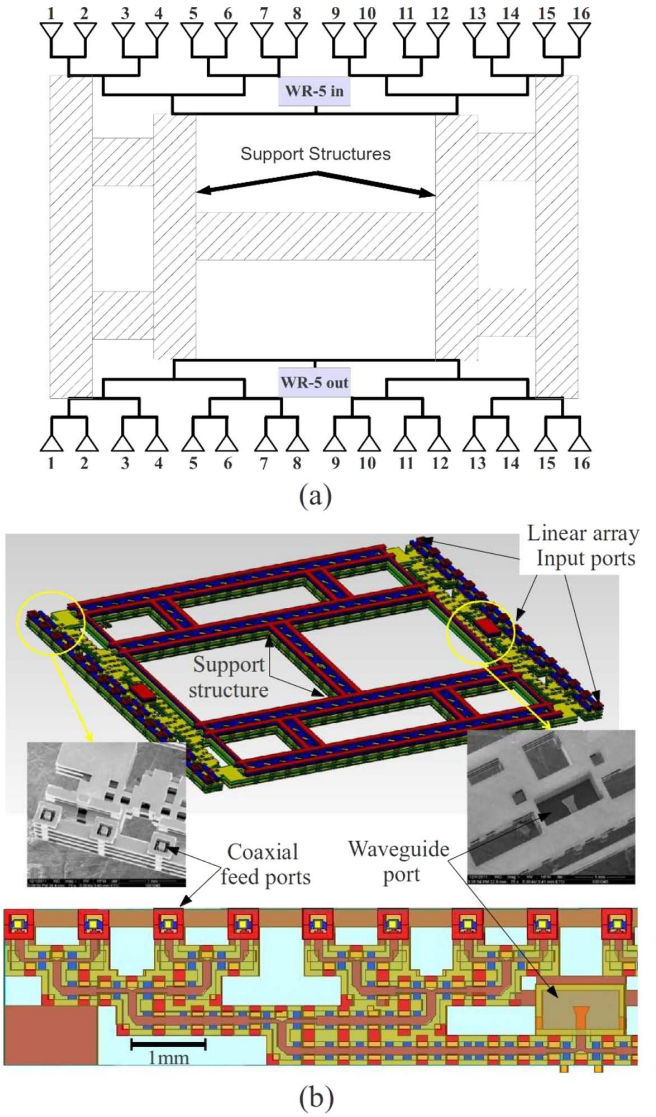

Fig. 5. Layout of the μcoaxial dividing network used as a feed for the 16 linear arrays each with 21 radiating slots. An identical dividing network was used to terminate the 16 arrays into a standard WR-5 matched load.

calculated as $1 - |S_{11}|^2 - |S_{21}|^2$. The results from the full-wave single-slot simulations where used in a circuit model to numerically optimize the design parameters for simultaneous impedance matching at the array terminations, high array radiation efficiency and specified array beam shape. In particular to design a uniform array the slot coupling in the final design was increased progressively for slot elements located further from the input port of the array. The final linear arrays were further simulated in HFSS™ for verification and further optimization.

In order to build the planar-array prototype, multiple linear arrays need to be fed in phase. The 1:16 μcoaxial feed shown in Fig. 5 was used for this purpose. The design is a standard 50 Ω corporate network with stepped impedances [18]. The feed has less than 9 dB of return loss from 130 to 155 GHz, as shown in Fig. 6 and it is terminated into a μcoaxial to waveguide vertical transition [19] with better than 10 dB of return loss from 130 to 180 GHz. The resonances visible in Fig. 6 are simulations artifacts and they were absent from the measured prototypes. The

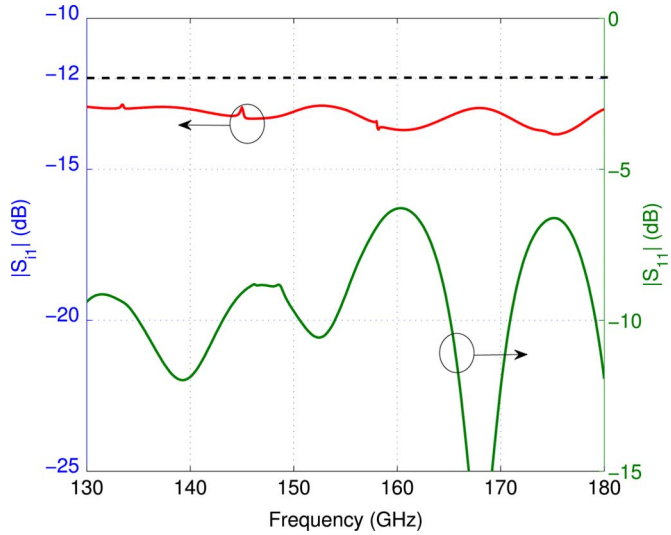

Fig. 6. Simulated transmission and return loss of the μ coaxial feed network. The feed network has better than 9 dB of return loss from 130 to 155 GHz. The simulation includes copper loss, which contributes to about 1 dB of loss relative to the -12 dB transmission coefficient value for a 1:16 divider. The simulation showed a spread of ± 0.5 dB in the transmission coefficients S_{i1} because of numerical errors.

same dividing network was used to terminate the arrays onto a single waveguide load. The array output port was terminated into a WR-5 transition that was used both to terminate the traveling-wave arrays and for S-parameter testing. An alternative solution including multiple micromachined loads to terminate the antenna arrays is also being investigated.

The μcoaxial-to-ridge waveguide transition shown in Fig. 7 was designed to connect the array to the feed network. The μcoaxial line is inserted through the bottom wall of the waveguide, while the center conductor is terminated above the waveguide ridge into a square section at 100 μm from the top wall. The distance between the transition and the waveguide back short as well as the size of the square termination were optimized for impedance matching. HFSS™ simulations show better than 12 dB of return loss for this transition from 130 to 180 GHz.

III. Device Fabrication

The device was fabricated in PolyStrata®, a photolithographically defined, sequential layer deposition process [14]. The μcoaxial lines and ridge waveguides were fabricated by depositing uniform layers of copper over a dielectric substrate and using a photoresist to define the μcoaxial shape. The thickness of each layer can range from 5 to 100 μm and up to 15 layers can be deposited. The specific layers used in this work are shown in Fig. 8. At the end of the process the photoresist was removed from the structure via release holes, leaving a low-loss, air-filled μcoaxial line or waveguide. In order to achieve optimum performance, the position of the release holes must be designed with minimal impact on RF performance, but with sufficient density to allow complete removal of the photoresist. During the fabrication process, small straps of a dielectric polymer are deposited to provide support for the coaxial center conductor, once the photoresist is released. For

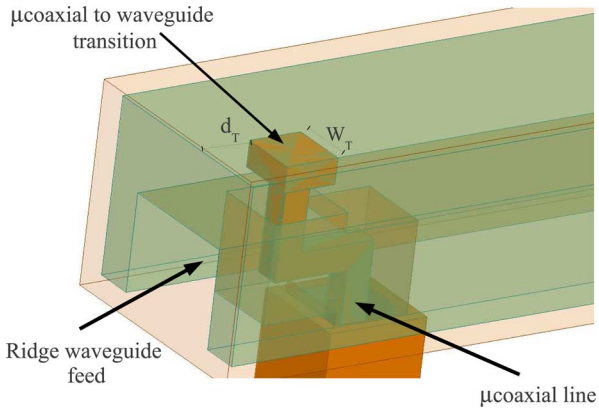

Fig. 7. Geometry of the μcoaxial to ridge waveguide transition. The μcoaxial inner conductor coming out of the ridge is terminated into a wider cap for impedance match. The size of the termination and the distance from the waveguide back-short is optimized for impedance match. The optimized dimensions were $w_T = 200$ μm and $d_T = 350$ μm.

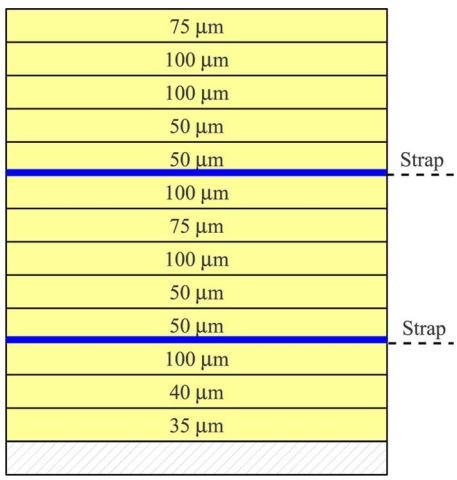

Fig. 8. Copper layer structure used in this work. The positions of the dielectric straps are indicated in blue.

the waveguide section the center line and dielectric straps are not needed, and it is straightforward to introduce corrugations in the bottom wall.

The release holes in the fabricated device were carefully placed to reduce the impact on the antenna radiation. The size of the release holes is 200 μm$\times$100 μm on the side wall. No release holes were required on the top wall, because the radiating slots act as release holes as well. The final 16$\times$21 element prototype, shown in Fig. 9, was mounted on a brass fixture with WR-5 waveguide through-vias to mate with standard waveguide flanges. A detail of the device is shown in Fig. 10.

IV. Experimental Results

The radiation patterns of the antenna array were characterized in a quasi-optical measurement setup [12], [20] shown in Fig. 11. A tunable Gunn diode oscillator followed by a frequency doubler was used as a source. The source output was radiated by a scalar feed horn, collimated by a lens and reflected by a mirror into a polarizing beam splitter. The resulting linearly polarized beam was sent to the array under test, terminated into a *G*-band detector. The array under test was mounted on

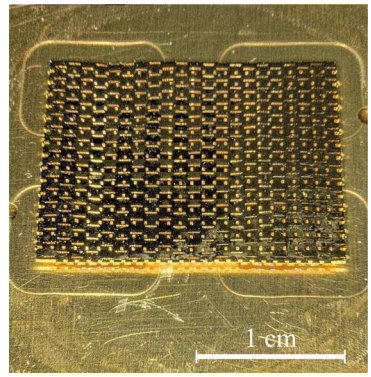

Fig. 9. Photograph of the fabricated 16$\times$21 elements scanning array prototype.

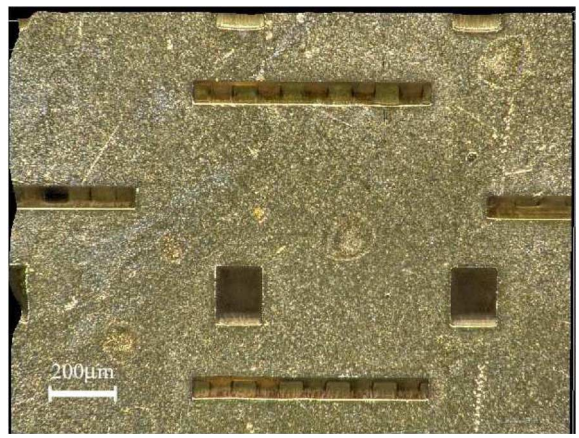

Fig. 10. Detail of the array prototype, showing the slots and the corrugated waveguide underneath.

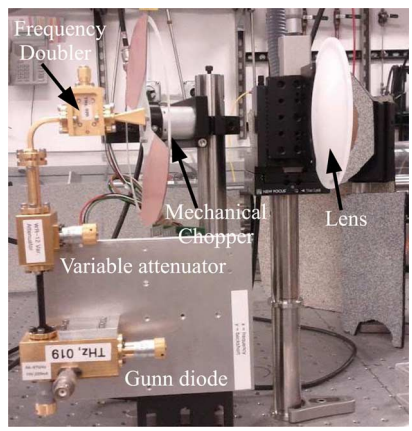

Fig. 11. Detail of the quasi-optical measurement setup for array radiation pattern measurements.

a computer-controlled azimuth-elevation stage for beam-scanning. The experimental setup is suitable to measure complex 2-D antenna patterns in both amplitude and in phase as discussed in [20]. However, in this work only the pattern amplitude was characterized.

To obtain the gain of the array under test, a calibration was performed by using a standard gain horn as a reference, as discussed in more detail in [12]. The horn used in this work had a nominal gain between 22 and 23.6 dBi in the 130–180 GHz range, as verified with HFSS® simulations.

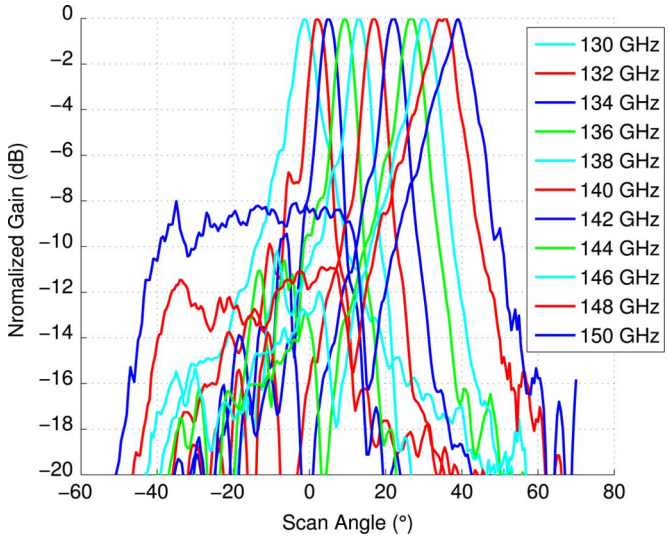

Fig. 12. Measured normalized H-plane beams for the 16×21 element array from Fig. 9.

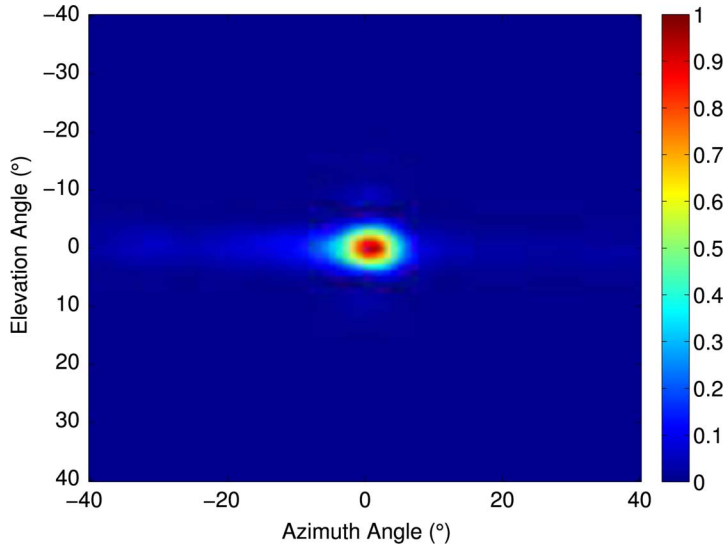

Fig. 14. Measured normalized 2-D radiation pattern plot at 130 GHz shown on a linear scale. The 3-dB beamwidth is 6° in the elevation plane.

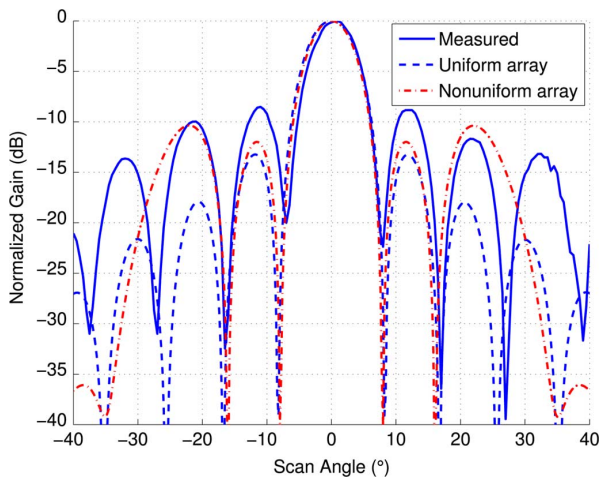

Fig. 13. Measured E-plane beam at 130 GHz for the 16×21 element array from Fig. 9. The dashed line is a simulation corresponding to the ideal case of a uniform in-phase excitation of each elementary linear array. The dot–dash line is a simulation for a nonuniform excitation caused by 12 dB input return loss for the linear arrays and the resulting standing wave.

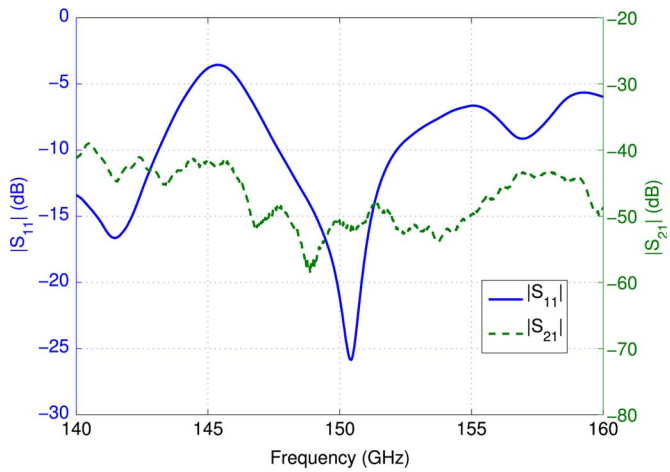

Fig. 15. Measured transmission and return loss for the 16×21 element array from Fig. 9. The transmission measurement shows that little power is dissipated into the load.

The fabricated prototype was tested and the measured beams from 130 to 150 GHz are shown in Fig. 12. The array scans from −1° to 39° from 130 to 150 GHz, resulting in a 2°/GHz scanning angle per unit frequency and in good agreement with the theoretical predictions and simulations. This is also twice the value that has been reported with a regular slotted waveguide array [12] in the same frequency range, thus requiring half the bandwidth for the VCO. The measured 3-dB beamwidth is about 6° wide in the elevation plane and 6.5° to 9° wide in the azimuth plane, depending on the frequency. A typical E-plane pattern is shown in Fig. 13. The beam scans mainly in the array H-plane, as expected, and moves by 5° at most in the E-plane. Full-wave simulations of the planar array were not possible, due to computational complexity, and therefore in Fig. 13 we compare the measured results with a linear array simulation multiplied by the appropriate (uniform) array factor. The difference in side lobes could be attributed to a nonuniform excitation due to impedance mismatch and, possibly, fabrication tolerances. The measured 2-D pattern at 130 GHz is plotted in Fig. 14 and shows a pencil beam, as expected.

The array S-parameters were measured with an Agilent PNA-X microwave network analyzer connected to Rohde and Schwarz millimeter-wave converters with a range of 140 to 220 GHz. Calibration was performed using a thru/offset short/short/match WR-5 kit. The array had less than 10 dB return loss from 130 to 143 GHz and from 147 to 160 GHz, as shown in Fig. 15. A peak in the reflected power is visible at 145 GHz and it is due to the μcoaxial feed network, seen also in Fig. 6. The measured gain and scan angle are shown in Fig. 16 and compared with HFSS™ simulations of a single linear array multiplied by an ideal array factor to obtain the planar device beams. Test structures were also measured to characterize and calibrate the losses in the feed. The measured results are in good agreement with the simulations (within 2 dB for the gain and within 0.5 ° for the scan angle). The measured patterns

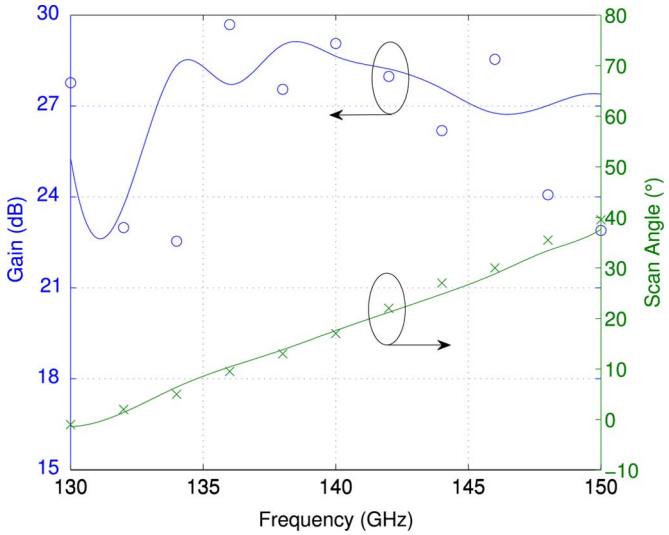

Fig. 16. Measured (markers) and simulated (continuous line) gain and scan angle for the array from Fig. 9.

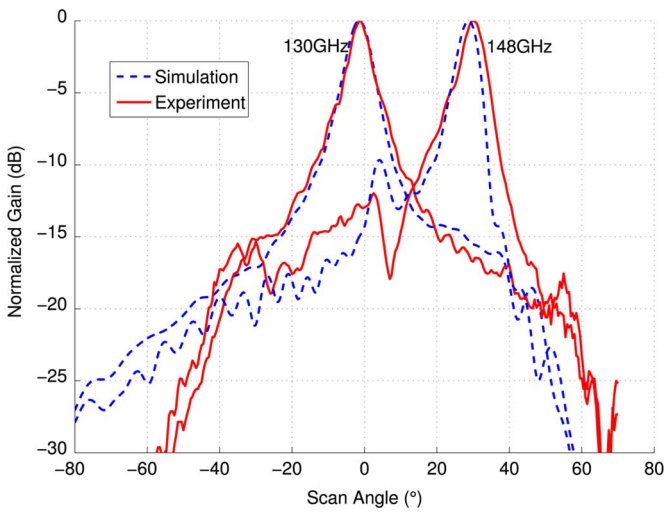

Fig. 17. Measured beams (continuous line) for the 16×21 element array from Fig. 9 at 130 and 148 GHz compared with full-wave simulations (dashed line).

at two typical frequencies are shown in detail in Fig. 17 and compared with the simulations.

V. Discussion and Conclusion

The traveling-wave slotted-waveguide array is scalable to some degree, since the number of elements is limited by the ability to obtain uniform excitation across the array length. In order to test the scalability of the design procedure in size as well as in frequency, we designed and fabricated a 5×5 cm array, shown in Fig. 18. The new device has 32×32 slots and operated between 150 and 180 GHz. The measured beams are shown in Fig. 19. The scanning angle is increased to about 60°, because of the increased bandwidth, while the scanning per unit frequency is about 2.1°/GHz. The beamwidth is now reduced to 3.2°, as can be predicted given the size of the array. However the new device is characterized by higher sidelobes, a consequence of the nonuniform excitation of the slot elements.

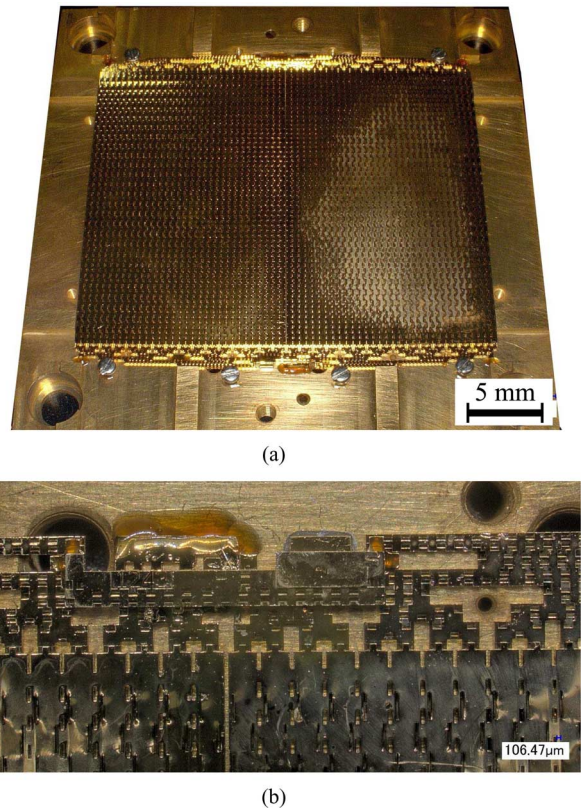

Fig. 18. (a) Photograph of the fabricated 32×32 elements scanning array prototype. (b) Detail of the corporate feed network.

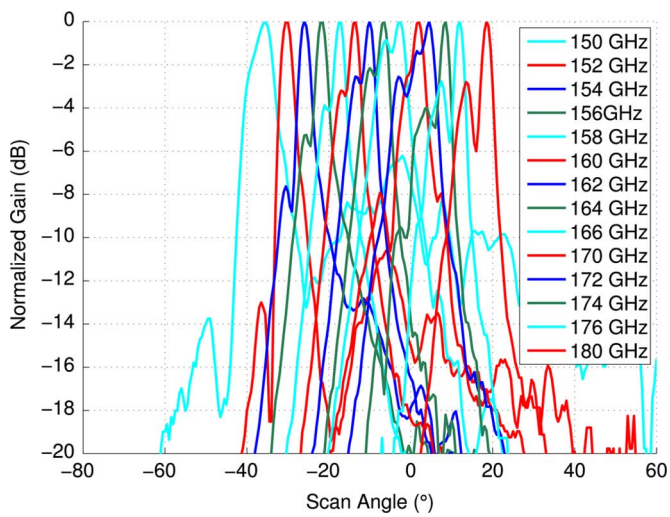

Fig. 19. Measured beams for the 32×32-element array from Fig. 18.

The gain and scan angle of the new device are shown in Fig. 20. In summary, in this work planar microfabricated slot antenna arrays operating at *G*-band have been discussed. A 2×2 cm antenna array having a scan angle of about 40° from 130 to 150 GHz with a 6° beamwidth was shown. A wide scan angle is obtained by periodically corrugating the ridge in the feed line in order to increase the signal dispersion in the band of interest. The array is fabricated in PolyStrata®, gold-plated and connected to a standard WR-5 flange through a custom fixture. The slot offsets are arranged to achieve an approximately

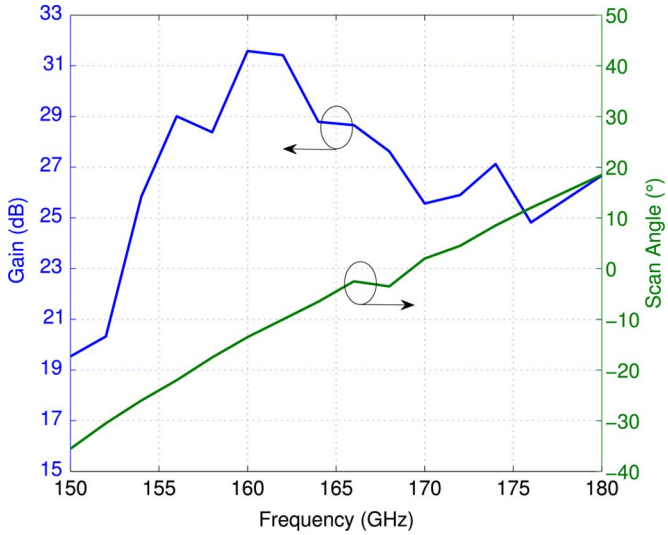

Fig. 20. Measured gain and angle for the 32×32 element array from Fig. 18.

uniform slot excitation and low sidelobes over the whole frequency range and a μ coaxial feed network is used to feed the planar array. The devices have potential applications to space exploration and planetary landing radar.

ACKNOWLEDGMENT

The authors extend their thanks to D. Novotny at NIST-Boulder, CO, USA, for his invaluable assistance measuring the S-parameters of the arrays.

REFERENCES

[1] R. Hansen, *Phased Array Antennas*, ser. Wiley Series in Microwave and Optical Engineering. Hoboken, NJ, USA: Wiley, 1998.
[2] B. Pollard, G. Sadowy, D. Moller, and E. Rodriguez, "A millimeter-wave phased array radar for hazard detection and avoidance on planetary landers," in *2003 IEEE Aerosp. Conf.*, Mar. 2003, vol. 2, pp. 1115–1122.
[3] B. Pollard and G. Sadowy, "Next generation millimeter-wave radar for safe planetary landing," in *2005 IEEE Aerosp. Conf.*, 2005, pp. 1213–1219, IEEE.
[4] B. Pollard and C. Chen, "A radar terminal descent sensor for the mars science laboratory mission," in *2009 IEEE Aerosp. Conf.*, 2009, pp. 1–10.
[5] A. Stehle, G. Georgiev, V. Ziegler, B. Schoenlinner, U. Prechtel, H. Seidel, and U. Schmid, "RF-MEMS switch and phase shifter optimized for W-band," in *38th Eur. Microw. Conf. (EuMC 2008)*, Oct. 2008, pp. 104–107.
[6] K. Sakakibara, , G. Kouemou, Ed., *Radar Technology*. : Intech, 2010 [Online]. Available: http://www.intechopen.com/books/radar-technology/high-gain-millimeter-wave-planar-array-antennas-with-traveling-wave-excitation
[7] L. A. Gustavson, Hughes Aircraft Co., Culver City, CA, USA, "S-band two-dimensional slot array," Tech. Memo 462, Mar. 1957.
[8] A. Derneryd and T. Lorentzon, "Design of a phase/frequency scanned array antenna with non-resonant slotted ridge waveguide elements," in *1991 AP-S. Dig. Antennas and Propag. Soc. Int. Symp.*, Jun. 1991, vol. 3, pp. 1728–1731.
[9] Y.-K. Fuh, A. Margomenos, Y. Jiang, and L. Lin, "Micromachined W-band plastic slot array antenna with self-aligned and integrated flange," in *2009 Int. Transducers, Solid-State Sensors, Actuators and Microsyst. Conf.*, Jun. 2009, pp. 2122–2125.
[10] B. R. Rao, "94 ghz slotted waveguide array fabricated by photolithographic techniques," *Electron. Lett.*, vol. 20, no. 4, pp. 155–156, 1984.
[11] P. James, "A waveguide array for an unmanned airborne vehicle (UAV)," in *11th Int. Conf. IEE Antennas Propag.*, Apr. 2001, vol. 2, pp. 810–813, vol. 2, IEE Conf. Publ. 480.
[12] E. Cullens, L. Ranzani, K. Vanhille, E. Grossman, N. Ehsan, and Z. Popovic, "Micro-fabricated 130–180 GHz frequency scanning waveguide arrays," *IEEE Trans. Antennas Propag.*, vol. 60, no. 8, pp. 3647–3653, Aug. 2012.
[13] A. Fackelmeier and E. Biebl, "Narrowband frequency scanning array antenna at 5.8 GHz for short range imaging," in *2010 IEEE MTT-S Int. Microw. Symp. Dig.*, May 2010, pp. 1266–1269.
[14] D. Sherrer and J. Fisher, "Coaxial waveguide microstructures and the method of formation thereof," U.S. Patent 7 012 489, Mar. 14, 2006.
[15] D. M. Pozar, *Microwave Engineering*, 3rd ed. Hoboken, NJ, USA: Wiley, 2005, pp. 423–430.
[16] R. E. Collins, *Field Theory of Guided Waves*, 2nd ed. Hoboken, NJ, USA: Wiley, 1990, pp. 605–.
[17] R. Elliott and L. Kurtz, "The design of small slot arrays," *IEEE Trans. Antennas Propag.*, vol. 26, no. 2, pp. 214–219, Mar. 1978.
[18] C. A. Balanis, *Antenna Theory: Analysis and Design*, 3rd ed. Hoboken, NJ, USA: Wiley, 2012, pp. 865–.
[19] J. Oliver, J.-M. Rollin, K. Vanhille, N. Barker, C. Smith, A. Sklavounos, D. Filipovic, and S. Raman, "A 3-D micromachined W-band cavity-backed patch antenna array with integrated rectacoax transition to waveguide," in *IEEE MTT-S Int. Microw. Symp. Dig.*, Jun. 2009, pp. 1641–1644.
[20] E. N. Grossman, A. Luukanen, and A. J. Miller, "Holographic microantenna array metrology," in *SPIE*, R. Appleby and D. A. Wikner, Eds., 2005, vol. 5789, no. 1, pp. 44–50.

Leonardo Ranzani (M'09) received the Ph.D. degree in information technology from Politecnico di Milano, Milan, Italy, in 2008.

From 2004 to 2009, he worked with the Consortium for Research in Optical Processing and Switching (Corecom), Milan, Italy. He is currently Research Associate at the University of Colorado at Boulder, CO, USA, and Research Affiliate at the the National Institute of Standards and Technology, Boulder, CO, USA. His research interests include microwave devices, DC-SQUID low noise cryogenic amplifiers, optics, and dispersion compensation.

Daniel Kuester (S'11) received the B.S.E.E. and B.M. degrees in 2007, and the Ph.D. degree in 2013, all from the University of Colorado in Boulder, CO, USA.

He is currently with Phase IV Engineering. From 2007 to 2012, he was with the National Institute of Standards and Technology, Boulder, CO, USA, under a research fellowship with the RF fields group in the electromagnetics division. His work has focused on metrology for wireless and THz, passive wireless sensing, small antennas, energy harvesting, and modulated scattering test and reliability.

Kenneth J. Vanhille (S'00–M'07) received the B.S. degree in electrical engineering from Utah State University in 2002, and the M.S. and Ph.D. degrees in electrical engineering from the University of Colorado at Boulder, CO, USA, in 2005 and 2007, respectively.

He is currently a Senior Member Technical Staff with Nuvotronics LLC, Durham, NC, USA. He has been technical and programmatic lead on many of the first commercialization efforts using the PolyStrata® microfabrication technology. His technical interests include high-frequency packaging techniques, millimeter-wave components and systems, and antenna design.

Anatoliy Boryssenko (M'98) received the M.S. and Ph.D. degrees in radio engineering systems from the Kiev Polytechnic Institute, Kiev, Ukraine.

Following his degree, he worked in R&D on ultra-wideband communication and sensing technologies, diverse electromagnetic systems across HF, VHF, VHF and microwaves, full-wave and asymptotic electromagnetic simulation and optimization software tools. He has worked till recently as a Research Professor at University of Massachusetts, Amherst, MA, USA. He is currently a Senior Member of Technical Staff at Nuvotronics LLC, Durham, NC, USA, where he is focused on R&D aspects of RF systems, antennas and phased arrays of microwave, millimeter and sub-millimeter wave bands.

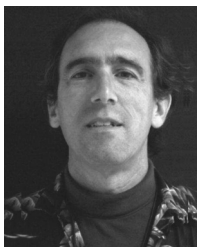

Erich N. Grossman received the A.B. degree in physics from Harvard College, Boston, MA, USA, in 1980, and the Ph.D. degree, also in physics, from the California Institute of Technology, Pasadena, CA, USA, in 1987. His thesis work involved development of an ultra-low noise, heterodyne receiver for 2 THz astronomy.

From 1988 to 1989, he was a Post-Doctoral Fellow at the University of Texas at Austin, and in 1989, he joined the National Institute of Standards and Technology, Boulder, CO, USA, where he is currently a physicist in the Optoelectronics Division. His work at NIST focuses on infrared and submillimeter system development. His notable accomplishments include the development and demonstration of the world's highest frequency, high efficiency lithographic antennas, the world's highest frequency Josephson junctions, and conception and early development of the SQUID multiplexer, first enabling large monolithic arrays of superconducting detectors. More recently, he has developed several 0.1–1 THz cameras for security applications.

Dr. Grossman was awarded a Department of Commerce Gold Medal in 1993. He is chair of the Metrology Working Group for the DARPA Terahertz Electronics program, and received the 2010 Allen V. Astin Measurement Science Award.

Zoya Popović (S'86–M'90–SM'99–F'02) received the Dipl.Ing. degree from the University of Belgrade, Serbia, Yugoslavia, in 1985, and the Ph.D. degree from the California Institute of Technology, Pasadena, CA, USA, in 1990.

Since 1990, she has been with the University of Colorado at Boulder, where she is currently a Distinguished Professor and holds the Hudson Moore Jr. Chair in the department of Electrical, Computer and Energy Engineering. In 2001, she was a Visiting Professor with the Technical University of Munich, Germany. Since 1991, she has graduated 44 Ph.D. students. Her research interests include high-efficiency, low-noise, and broadband microwave and millimeter-wave circuits, quasi-optical millimeter-wave techniques for imaging, active antenna arrays, and wireless powering for batteryless sensors.

Prof. Popovic was the recipient of the 1993 and 2006 Microwave Prizes presented by the IEEE Microwave Theory and Techniques Society (IEEE MTT-S) for the best journal papers, and received the 1996 URSI IssacKoga Gold Medal. She was the recipient of a 2000 Humboldt Research Award for Senior U.S. Scientists from the German Alexander von Humboldt Stiftung. She was elected a Foreign Member of the Serbian Academy of Sciences and Arts in 2006. She was also the recipient of the 2001 Hewlett-Packard (HP)/American Society for Engineering Education (ASEE) Terman Medal for combined teaching and research excellence.